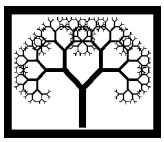

Proceedings of the Fourth International Conference
on Engineering Computational Technology,
B.H.V. Topping and C.A. Mota Soares (Editors),
Civil-Comp Press, Stirling, Scotland.

Paper 98

Assembly Synthesis for Stiffness, Dimensional Adjustability and Manufacturability

N. Lyu, B. Lee and K. Saitou
Department of Mechanical Engineering
University of Michigan, Ann Arbor, United States of America

Abstract

A method that identifies the optimal components set, joint designs and corresponding subassembly partitioning for a Body-In-White (BIW) made of the aluminium space frame (ASF) is presented where the structural stiffness, dimensional integrity and components manufacturing / assembly cost are considered as the objectives. The optimization problem is posed as a simultaneous determination of the location and types of joints in a structure selected from the predefined joint library combined with the size optimization for the cross sections of the joined structural frames. The join library is a look-up table containing following three components: 1) the geometry of the feasible joints at each potential joint location, 2) the cross sectional designs of the joined frames and 3) the structural characteristics as the equivalent torsional spring models. Structural stiffness of the entire structure is evaluated by finite element analyses of a beam-spring BIW model constructed based on the joints and joined frames. The dimensional integrity of the assembly is calculated by evaluating how easily the adjustment of the critical dimensions in the structure can be achieved during the assembly process. Finally, manufacturing cost and assembly costs are estimated by considering the manufacturing and assembly procedures based on the geometries of the components and joints. The optimization problem is solved by multi-objective evolutionary algorithms using a graph-based crossover operator. The BIW of a middle size passenger car is decomposed as the case study where the representative optimal designs are selected from the resulting Pareto front and trade-offs among stiffness, dimensional integrity and manufacturing/assembly cost are discussed.

Keywords: structural design, assembly design, design for manufacturing, design for assembly, multi-objective optimization, genetic algorithms, cost estimation.

1 Introduction

The structures of large-scale mechanical products, such as ships hulls, airplanes and automotive bodies, are fairly complex that it is almost impossible (or too expensive) to be manufactured in one piece. Therefore, in general, these products are assembled with hundreds of components. Hence, during the conceptual stage of designing such products, designers need to decompose the entire product geometry into the set of components and assign joints among those components. Industry practices do not come up to systematic approaches, whereas the effect of this process on following properties of the assembled product is significant:

- Overall structure stiffness
- Manufacturing and/or assembly cost
- Dimensional integrity

Therefore, introducing a cost-effective but systematic optimization method in determining the components set considering overall structural stiffness, manufacturing and assembly costs, and dimensional integrity altogether will have a significant impact on the industries.

Assembly synthesis has been defined by Yetis and Saitou [1] as the decomposition of the end product design prior to the detailed component design phase in the systematic ways. This paper integrates our previous works on the decomposition-based assembly synthesis methods [2-6], by considering the stiffness, the manufacturing / assembly cost [3, 4], and the dimensional integrity [2, 6] altogether in finding optimal assembly syntheses. To solve the optimization problem posed with multiple objectives, a multi-objective genetic algorithm (GA) [7] with a direct crossover operator [8, 9] is used. The GA synthesizes candidate assembly designs by selecting joints from a predefined set of joint types (*i.e.*, joint library [5]) for predefined potential locations, thus defining component set, deciding the beam cross sections and welding thickness where joints are assigned. Then all objectives are evaluated for each candidate assembly design.

Structural characteristics of an assembly are evaluated by finite element analyses of a model made of beam elements (frames) and torsional spring elements (joints), constructed with the selected joints and joined frames. Manufacturing/assembly cost is evaluated based on the estimated costs of the manufacturing/assembly procedures, including the costs of extrusion die, bending operation, casting component for each joint and welding costs in the assembly process. Dimensional integrity of the assembly is estimated by checking if critical dimensions are adjustable during assembly processes. In the large-scale structural assembly, tolerance level of critical dimensions (or Key Characteristics; KCs) required on the final assembly is usually tighter than tolerance level of typical component fabrication methods when accumulated. For this reason, KCs are adjusted on fixtures and the joints between relative components or subassemblies are fastened. In doing so, it is important to have joints allowing a small amount of relative motion along the direction of the KC at the very assembly step where the KC is being achieved. For example, see Figure 1,

which shows a simplified car floor pan design [10]. Suppose total length is a KC, then there should be at least a joint allowing the adjustment along the KC on the fixture. However, a poor assembly sequence (Figure 1 (a)) does not allow such adjustability because the joint at the second step (where KC is being achieved) can not absorb the variation of component 1. It is obvious that, dissimilar to the other objectives, the adjustability for KCs can not be evaluated without considering assembly sequences. For this reason, in-process dimensional adjustability is evaluated through a nested optimization routine, where the assembly sequence yielding the best adjustability is identified, for each assembly design generated by GA (refer to [2] for more details).

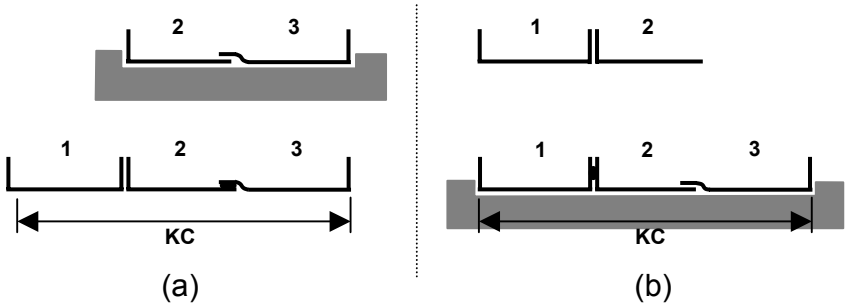

Figure 1: Assembly sequences (a) without and (b) with in-process adjustability.

The BIW of a middle size passenger vehicle is synthesized into an assembly in the case study, where the representative designs are selected from the resulting Pareto front and trade-offs among stiffness, manufacturing/assembly cost and dimensional integrity are discussed.

2 Approach

This section describes our method for synthesizing multi-components aluminium space frame using the joint library, which simultaneously identify the optimal components set and component/joint designs considering the stiffness of the assembled structure, manufacturing/assembly cost and dimensional integrity. The method consists of the following three major steps:

1. Geometry of the entire structure is transformed into a *structural topology graph*, representing the liaisons between *basic members*, the smallest decomposable components of the given structure, identified by the potential joint locations specified by the designer.
2. The product topology graph is decomposed into subgraphs representing components by using a set of joints in the joint library, thus generating candidate assembly designs.
3. Each candidate assembly design is evaluated for the criteria described above.

Three steps above are described in detail, in the rest of this section with an exemplary space frame structure shown in Figure 2. As illustrated in Figure 2 (b), it is assumed that frames are extruded tubes, bent or welded with cast "sleeves" at joints, following a typical construction method of the ASF.

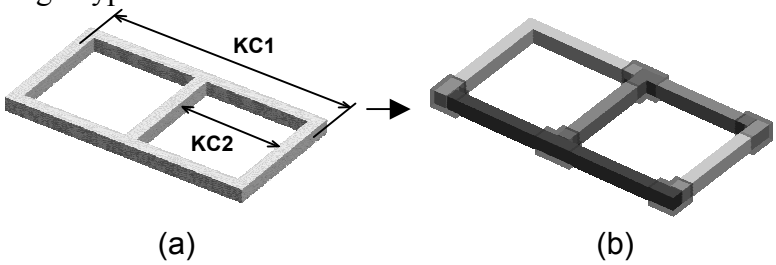

Figure 2: (a) A sample beam frame structure and (b) a possible components set.

2.1 Step 1: Construction of Structural Topology Graph

The presented method assumes that a human designer decides potential joint locations, thus defining basic members of the structural topology graph. As the basic member is allowed to be a separate component, when defining, one should consider the manufacturability of basic members according to the area of application.

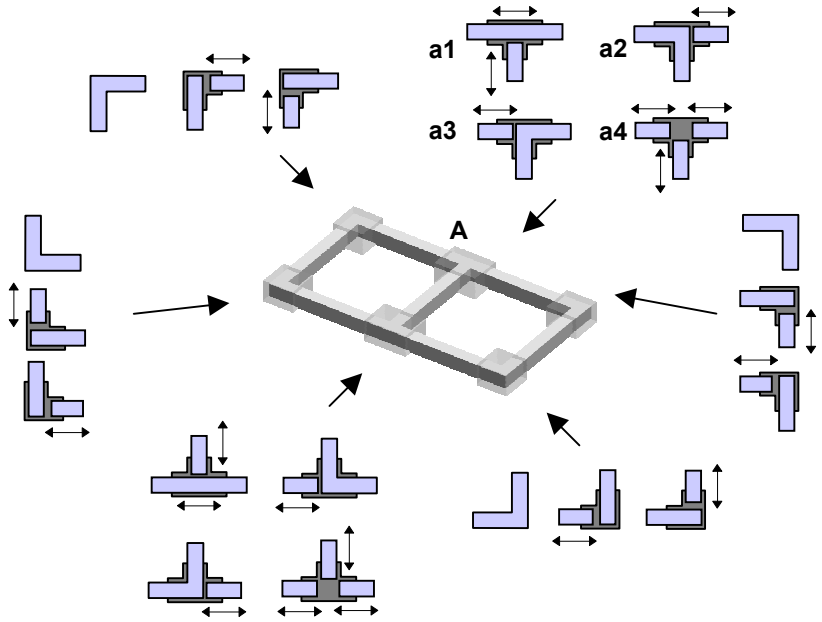

Figure 3: Specified potential joint locations (shown as grey boxes) and the joint library for each location. Arrows at each joint represent adjustable directions.

Figure 3 illustrates an example of six potential joint locations indicated by grey boxes. At each potential joint location, the designer is also required to specify (potentially different) feasible joint types to be included in the joint library. For

example, four joint types (**a1**~**a4**) are assumed as available at location **A** in Figure 3. Each joint type is associated with the joint design variables for the cross section of the joined frames and the amount of welds, with which the structural properties of a joint are determined as described in the following section.

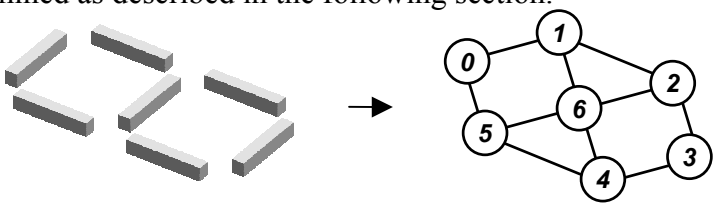

(a) (b)

Figure 4: (a) Basic members and (b) structural topology graph

The basic members can be identified from the specified potential joint locations (Figure 4, (a)). Then, the structural topology graph $G = (M, T)$ is constructed from the basic members (Figure 4, (b)) such that:

- Basic member m_i is represented as a node n_i in the node set M.
- The liaison between two basic members m_i and m_j is represented as edge $e = \{n_i, n_j\}$ in the edge set T.

As illustrated in Figure 4, a structural topology graph G (Figure 4, (b)) with 7 nodes corresponding to the seven basic members (Figure 4, (a)) and 10 edges connecting the adjacent nodes is constructed.

2.2 Step 2: Decomposition of Structural Topology Graph

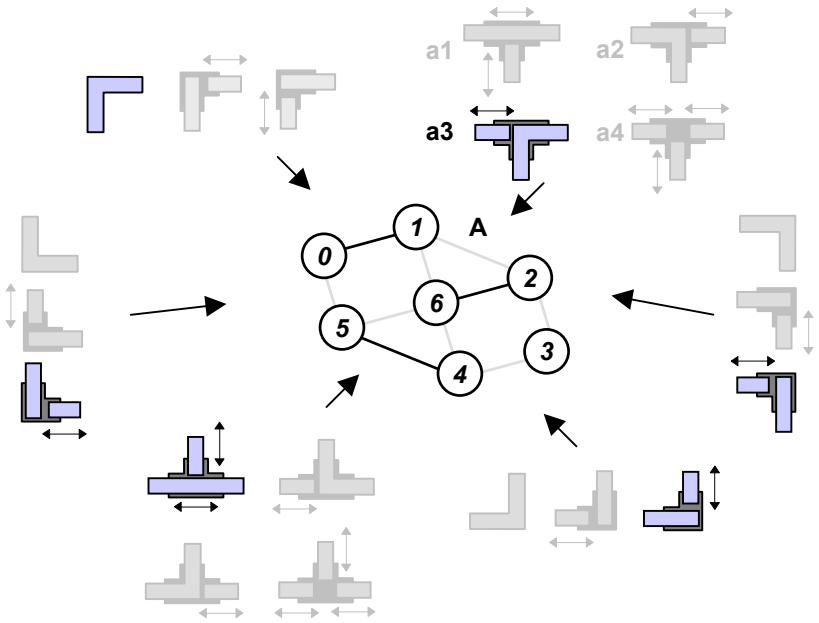

Figure 5: Selected joint types and corresponding topology graph modified

The structural topology graph *G* is decomposed by selecting a joint type in the library at each potential joint location. Based on the selected joint types, the corresponding edges in *G* are removed and *G* is decomposed into subgraphs. For example, by selecting joint type **a3** in the joint library for location **A** in Figure 5, the corresponding edges {1,2} and {1,6} are removed. The selection of joint types and the removal of the corresponding edges in *G* result in subgraphs of *G*, each of which corresponds to a component. The cross sectional dimensions of a component are then set as the averages of the ones in the joining frames (basic members) associated with the selected joint types in the component, which are subsequently used for retrieving the pre-computed structural properties of the joints from the joint library. Figure 6, for example, shows 4 subgraphs (Figure 6 (a)) and the corresponding components (Figure 6 (b)) resulted from the selection of the joint types in Figure 5.

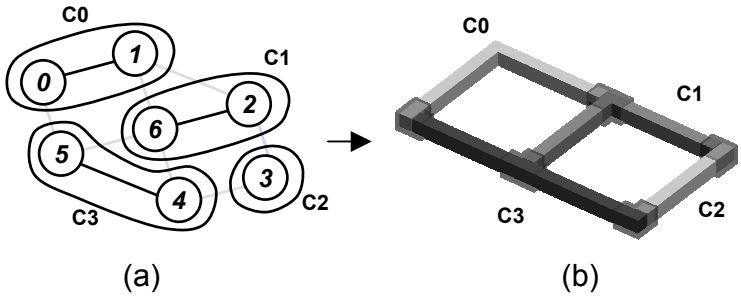

Figure 6: (a) 4 subgraphs and (b) corresponding 4 components

2.3 Step 3: Evaluation of an assembly design

Within an optimization loop, an assembly design consisting of components and joints obtained with above methods is evaluated based on 1) stiffness of the assembled structure, 2) manufacturing/assembly cost of the extruded components, cast "sleeves" for joints and selected joining operations, and 3) dimensional integrity.

2.3.1 Structural Stiffness

The structural stiffness of the assembled structure is evaluated as a negative of the magnitude of the displacements at specific locations of the assembled structure under given loading conditions. The displacements are calculated with finite element analyses, where the components and joints are represented by beam elements and torsional spring elements, respectively. For example, the structure with 4 beam components in Figure 7 (a) is modelled as beam-spring FE model in Figure 7 (b). The component cross section designs are used to estimate the cross sectional properties of the FE elements. T-joint in Figure 7 (a) is modelled as three beam elements connected by torsional spring elements k_0, k_1, and k_2, each of which has torsional stiffness (rate) around three local orthogonal axes attached to the joint. Note that the relative translations of these elements are constrained. The rate of the torsion spring elements are estimated by the finite element analyses of the detailed

model of the joint, where frames are modelled with plate elements, the cast sleeve is modelled as solid elements, and welds joining the frames and sleeve are modelled as plate elements.

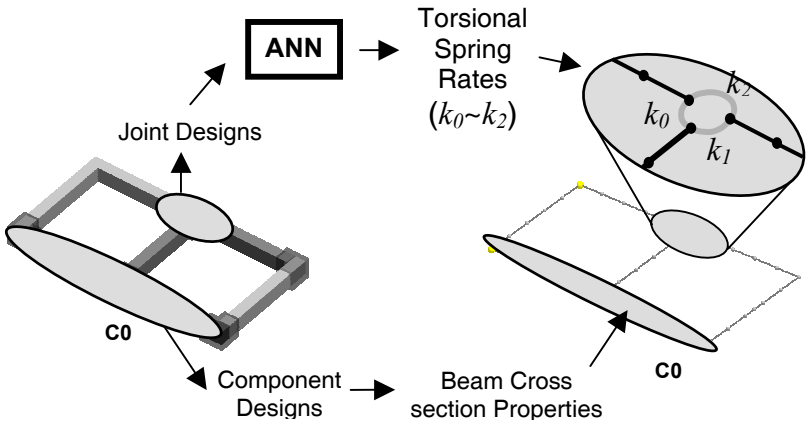

Figure 7: (a) Sample structure with 4 beam components and (b) FE model of (a).

The values of the torsional spring rates for typical joint types, cross sectional dimensions of the joined frames, and amount of welds are pre-computed to produce a set of training data for an Artificial Neural Network (ANN) that implements the joint library. Similar to the translator A of [11], this approach allows the spring rates of a joint can simply be retrieved from the ANN without computational overheads.

2.3.2 Dimensional Integrity

Dimensional integrity of the given assembly design is evaluated by estimating the in-process adjustability for the given KCs. In order to do this, an internal optimization routine is conducted, computing the subassembly partitioning for optimal in-process adjustability by solving the equivalent minimum cut problem on the weighted graphs. The approach is adopted from [2].

First, a configuration graph, $C = (M, T, A)$, is obtained by adding A, the set of edges representing KCs, on the structural topology graph $G = (M, T)$ (see Figure 8 (b)). Note that two KCs (Figure 8 (a)) are represented as two double-lined edges {0,3} and {3,6} in C. With assigned joints, the configuration graph is transformed to a liaison graph $L_0 = (V_0,E_0,A_0)$ as in Figure 8 (d), where V_0 is the set of nodes representing components, E_0 is the set of edges representing joints and A_0 is the set of edges representing KCs. The A_0 takes over all the KCs from the A, but connecting the nodes in V_0 that are hyper-nodes of the nodes in M (since a component can consist of one or more nodes). The assembly represented as L_0 is evaluated for in-process adjustability by the subsidiary routine for subassembly partitioning (Figure 9), until all KCs are broken, to check if adjustability is guaranteed for all KCs. Then the reverse of this subassembly partitioning yields a partial assembly sequence providing adjustability for all KCs.

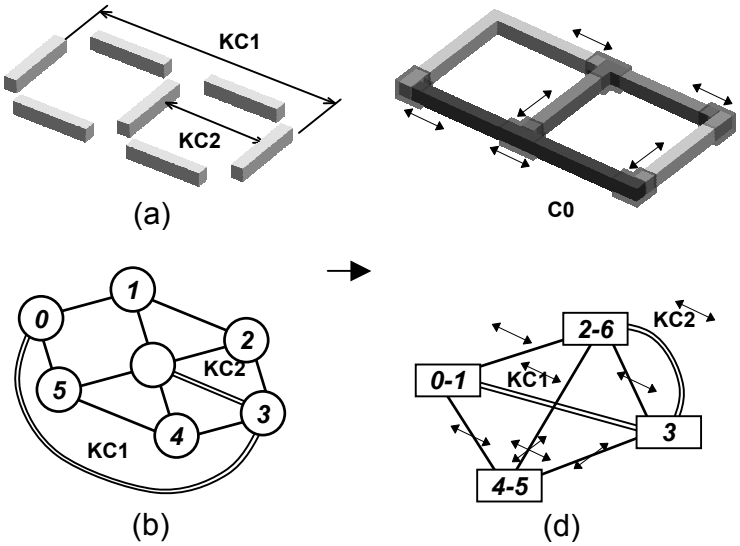

Figure 8: (a) Basic members and (b) corresponding configuration graph $C = (M, T, A)$. (c) A sample components set and (d) corresponding liaison graph L_0.

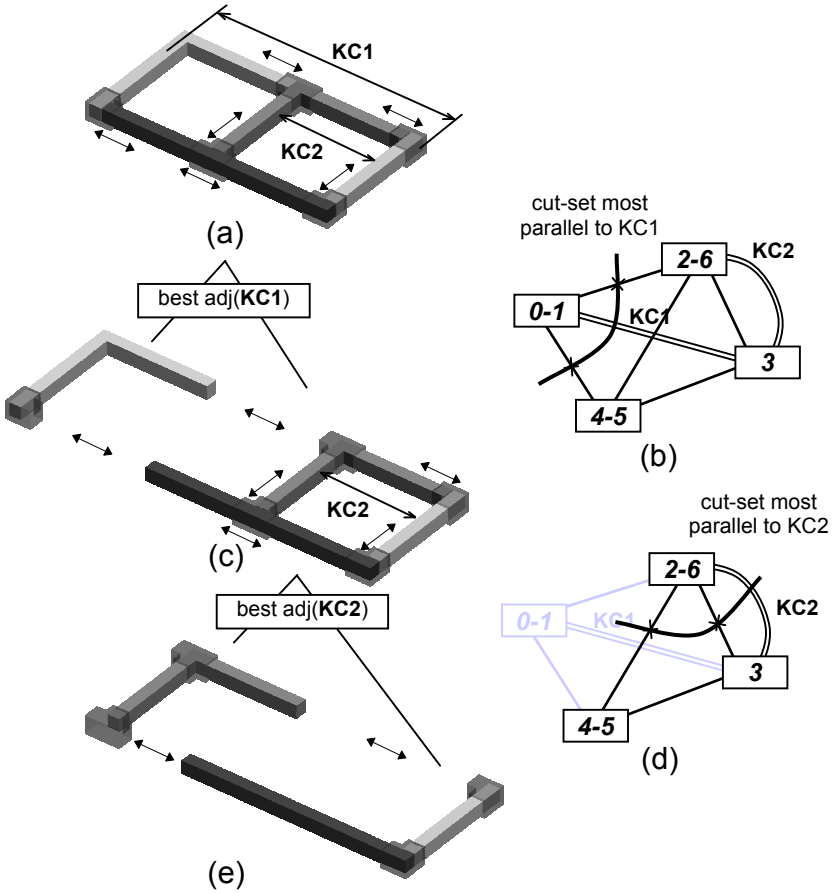

Figure 9: Partitioning with best adjustability

Figure 9 illustrates two-step partitioning of the given assembly (Figure 9 (a)), where the first partitioning (Figure 9 (b)) cut two edges {0-1,2-6} and {0-1,4-5} in L_0 to satisfy the **KC1**, resulting two sub assemblies shown in Figure 9 (c). The second partitioning (Figure 9 (d)) is done by cutting two edges {2-6,3} and {2-6,4-5} to satisfy **KC2**. Each partitioning is done by finding the optimal cut-set of edges whose adjustable directions are most parallel to the KC.

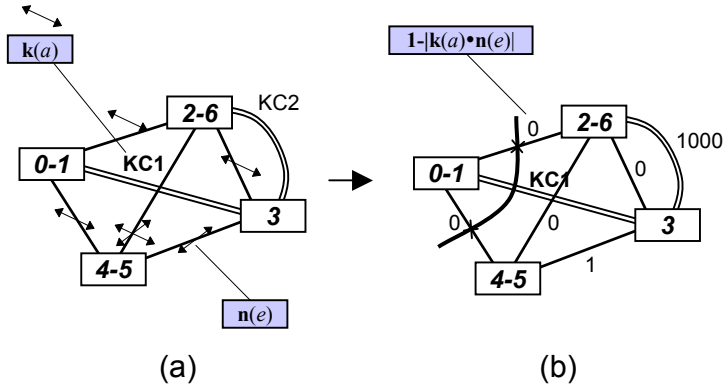

Figure 10: Details of the first partitioning in Figure 9.

Figure 10 illustrates details of the first partitioning in Figure 9. To find the optimal cut set, directional unit vectors are assigned to the edges in the liaison graph (**k**(a) for KC and **n**(e) for each edge e in Figure 10 (a)). Then the weight of each edge is defined and assigned as:

$$1-\left|\mathbf{k}(a)\bullet\mathbf{n}(e)\right| \tag{1}$$

The weight calculated from the Equation (1) will yield 0 if the joint on e has the perfect adjustability (parallel to) the KC, a. A joint with imperfect adjustability (non-parallel to KC) will have a positive weight less than 1 measuring their counter-adjustability. The optimal cut set to satisfy the given KCs will be obtained by finding the cut-set of edges whose weights minimize the following equation:

$$\sum_{a\in KC_p}\sum_{e\in CS_p}\left(1-\left|\mathbf{k}(a)\bullet\mathbf{n}(e)\right|\right) \tag{2}$$

, where a is the KC in the KC_p, the set of KCs broken by the partitioning p, and e is a joint in CS_p, the cut-set edges by the partitioning p. The formulation transforms the problem into the well-known minimum cut problem, for which many algorithms are available. Figure 10 shows the partitioning p with KC_p = {**KC1**} and CS_p = {{0-1,2-6},{0-1,4-5}} resulting in the minimum value of equation (2) as 0.0 (perfect adjustability: all joints in {0-1,2-6} and {0-1,4-5} are parallel to the **KC1**). Figure 11 illustrates the binary tree representing the subassembly partitioning in Figure 9. Each end node in the binary tree represents a subassembly consisting of one or more component(s). The adjustability over the entire subassembly partitioning is obtained simply by the summing up the values from Equation (2) for all partitions.

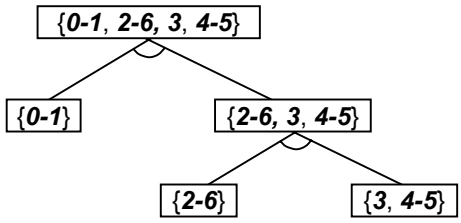

Figure 11: Binary Tree of the subassembly partitioning illustrated in Figure 9.

2.3.3 Manufacturing/Assembly Cost

The manufacturing cost of components is evaluated as a negative of the total cost of producing components. As stated earlier, it is assumed that frames are extruded tubes, bent or welded with cast "sleeves" at joints, following a typical construction method of aluminium space frames (ASF). For example, the design in Figure 12 (a) is composed of four frames (Figure 12 (b)) and 5 cast sleeves (Figure 12 (c)). The cost of producing components is estimated by the sum of the cost of extrusion die (assumed as proportional to the size and complexity of the frame cross sections) and the cost of bending operations (assumed as proportional to the number of bending). The cost of producing cast sleeves is estimated by the cost of casting, which is assumed to be proportional to its volume.

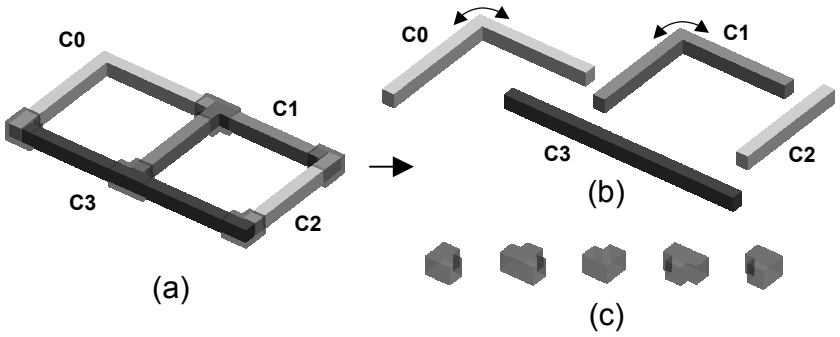

Figure 12: (a) Sample design, (b) 4 components with 2 bends (indicated as arc-arrows), and (c) 5 cast sleeves for joining.

The assembly cost is calculated as a negative of the total cost of joining. In this paper, the method of joining is assumed to be the GMAW (Gas Metal Arc Welding), which is widely used for ASF [12]. The welds are applied between the frames and the cast sleeves at joints. The cost is assumed to be proportional to the volume of total welds, which can be calculated from the total welding length multiplied by weld thickness. Total manufacturing/assembly cost is calculated from the summation of manufacturing cost and assembly cost.

3 Mathematical Formulation

3.1 Definition of Design Variables

A design is uniquely specified by 1) the joint types at all possible joint locations, 2) the cross sectional dimensions of all basic members, and 3) the amount of welds at all joints, which are represented by three vectors $\boldsymbol{x}$, $\boldsymbol{y}$, and $\boldsymbol{z}$, respectively:

$$\begin{aligned} \boldsymbol{x} &\in J_1 \times J_2 \times \cdots \times J_n \\ \boldsymbol{y} &\in S^B \\ \boldsymbol{z} &\in W^n \end{aligned} \tag{3}$$

where

- n is the number of possible joint locations in the structure,
- B is the number of basic members in the structure,
- J_i is the set of feasible joint types at the i^{th} possible joint locations,
- S is the set of feasible cross sectional dimensions,
- W is the set of feasible amount of welds.

Note the elements of vectors $\boldsymbol{y}$ and $\boldsymbol{z}$ can also be vectors depending on the definitions of S and W, as appeared in the following case study.

3.2 Definition of Objective Functions

Using the design variables $\boldsymbol{x}$, $\boldsymbol{y}$, and $\boldsymbol{z}$, the three objective functions described in the previous section are given as follows:

$$f_{stiff}(\boldsymbol{x},\boldsymbol{y},\boldsymbol{z}) = -\mathrm{DISP}(\mathrm{XSEC}(\boldsymbol{x},\boldsymbol{y}),\mathrm{JRATE}(\mathrm{XSEC}(\boldsymbol{x},\boldsymbol{y}),\boldsymbol{z})) \tag{4}$$

$$f_{mfg,assm}(\boldsymbol{x},\boldsymbol{y},\boldsymbol{z}) = f_{mfg}(\boldsymbol{x},\boldsymbol{y}) + f_{assm}(\boldsymbol{z}) \tag{5}$$

$$f_{adj}(\boldsymbol{x}) = -\sum_{p\in P(x)}\sum_{a\in KC_p}\sum_{e\in CS_p}\left(1-\left|\mathbf{k}(a)\bullet\mathbf{n}(e)\right|\right) \tag{6}$$

, where

$$f_{mfg}(\boldsymbol{x},\boldsymbol{y}) = -\sum_{i=0}^{n-1}\left\{\mathrm{DIEC}(\mathrm{COMP}(i,\boldsymbol{x}),\boldsymbol{y}) + \mathrm{BNDC}(\mathrm{COMP}(i,\boldsymbol{x}))\right\} - \sum_{i=0}^{m-1}\mathrm{CASTC}(i,\boldsymbol{x}) \tag{7}$$

$$f_{assm}(z) = -C_w\sum_{i=0}^{m-1}\mathrm{WLDL}(i,\boldsymbol{z})\times\mathrm{WLDT}(i,\boldsymbol{z}) \tag{8}$$

and

- n and m are the numbers of components and joints in a decomposed structure, respectively.
- DISP is the amount of displacements at predefined points of the beam-torsional spring FE model of assembled structure.
- XSEC($\boldsymbol{x}$, $\boldsymbol{y}$) is the cross sectional properties of the components specified by $\boldsymbol{x}$ with the beam cross sectional dimensions specified by $\boldsymbol{y}$.
- JRATE is the torsional spring rates at each joint with cross sectional properties XSEC and weld amount $\boldsymbol{z}$.
- COMP(i,$\boldsymbol{x}$) is the i^{th} component specified by $\boldsymbol{x}$.
- DIEC and BNDC are the cost of extrusion die and bending operation of a component, respectively.
- CASTC(i,$\boldsymbol{x}$) is the casting cost at the i^{th} joint specified by $\boldsymbol{x}$.
- C_w is the cost of welding operation per unit weld volume.
- WLDL(i,$\boldsymbol{z}$) and WLDT(i,$\boldsymbol{z}$) are the length and thickness of the welds at the i^{th} joint as specified by $\boldsymbol{z}$.
- $P(\boldsymbol{x})$ is a subassembly partitioning for the assembly design defined by $\boldsymbol{x}$.
- KC_p is the set of KCs of the partitioning p.
- CS_p is the cut-set edges in the partitioning p.
- a is the KC in the KC_p and e is a joint in CS_p.
- $\mathbf{k}(a)$ and $\mathbf{n}(e)$ are normal vector for a and e, respectively.

3.3 Optimization Problem

Given the design variables and the objective functions as define above, the following multi-objective optimization problem is formulated:

maximize: $\left\{f_{stiff}(\boldsymbol{x},\boldsymbol{y},\boldsymbol{z}), f_{mfg,assm}(\boldsymbol{x},\boldsymbol{y},\boldsymbol{z}), f_{adj}(\boldsymbol{x})\right\}$

subject to:

$$\boldsymbol{x} \in J_1 \times J_2 \times \cdots \times J_n$$
$$\boldsymbol{y} \in S^B$$
$$\boldsymbol{z} \in W^n$$

Note that there is no explicit constraint in this problem.

A modified Non-Dominated Sorting Genetic Algorithm-II (NSGA-II) [7] is adopted for the above problem due to the discrete nature of the design variables, and its ability to solve multi-objective problems without predefined weight or bounds. Some enhancements to the conventional NSGA-II are made in the niching based on the distances in object function space and the stochastic universal sampling, which was successfully applied in our previous work [9].

A chromosome $\boldsymbol{c}$ (an internal representation of design variables for GA) is a simple list of the 3 design variables:

$$\boldsymbol{c} = (\boldsymbol{x}, \boldsymbol{y}, \boldsymbol{z}) \tag{9}$$

Since the information in ***x***, ***y***, and ***z*** are linked to the physical geometry of structure, the conventional one point or multiple point crossover for linear chromosomes [13] are ineffective in preserving high-quality building blocks. For this type of problems, direct crossover has been successfully applied to improve the performance [8, 9], whose details can be found in [3] along with the description of the modified NSGA-II.

4 Case Study

This section presents a case study on a model of aluminium space frame (ASF) of a passenger vehicle shown in Figure 13. The actual vehicle design (Figure 13 (a)) is first simplified (Figure 13 (b)), where all frames are assumed as square tubes with identical external dimensions and with possibly different internal thicknesses. Since the actual vehicle body is a mixture of extruded and cast parts, only the portions corresponding to the extruded parts are subject to decomposition in the simplified model. Assuming the symmetric components in the left and right sides of the body, the design variables are assigned to only one side of the simplified model.

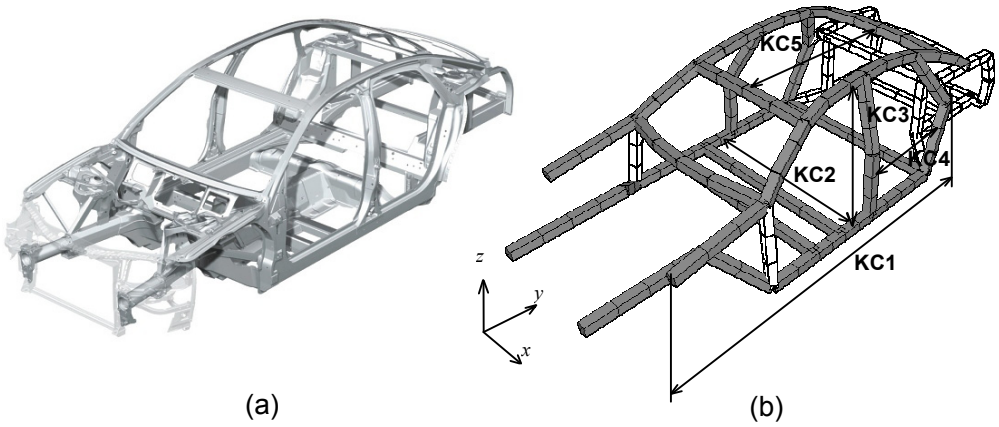

Figure 13: (a) ASF for a medium size passenger car and (b) simplified frame model used in the case study with 5 KCs (**KC1**~**KC5**).

Table 1 shows the material properties used in this case study. Total of 30 potential joint locations are specified as shown in Figure 14 (a). These potential joint locations are classified into three types A, B, and C, each of which has feasible joint types shown in Figure 14 (b) with 90 or 180 degree angles between the joined frames. Location type A has two joint types, **a0** and **a1**. In **a0**, beams 0 and 1 are one component ((0,1)) while in **a1**, beams 0 and 1 are welded with cast sleeve ((0),(1)). Location type B has three configuration designs **b0**, **b1**, **b2**. In **b0**, beams 0 and 2 is one component, joined to 1 ((0,2),(1)). Similarly, **b1** and **b2** have two components ((0,1),(2)) and ((0),(1,2)), respectively. For location type C, **c0**, **c1** and **c2** have joint types ((1,2),(0)), ((1),(0,2)), and ((0,1),(2)), respectively

Process	*Name*	*E**	*Poisson's Ratio*	*Density***
Extrusion	A6061-T6	70.5	0.33	2700.0
Casting	A356.0-T6	72.4	0.33	2685.0
Welding	A4043	70.5	0.33	2700.0

*E: Young's Modulus [GPa], ** Density: [Kg/m^3]

Table 1: Material Properties in ASF model

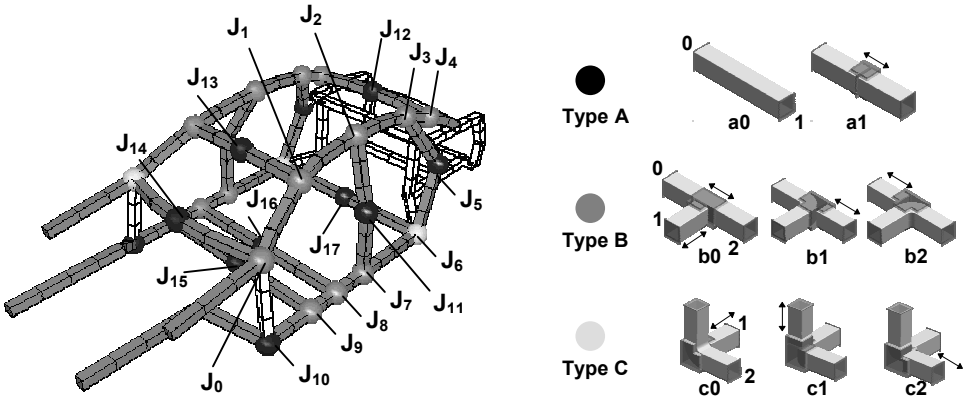

(a) (b)

Figure 14: (a) Potential joint locations and (b) possible configurations (joint library) for each joint type. Arrows in (b) indicate the adjustable directions.

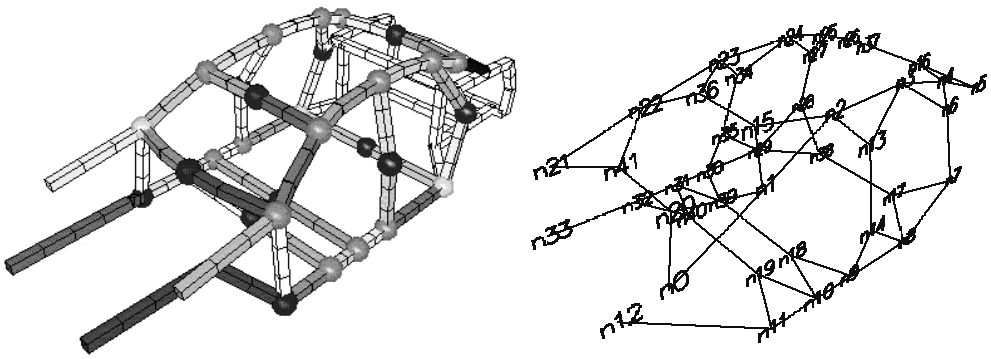

(a) (b)

Figure 15: (a) Basic members and (b) constructed structural topology graph

Based on the specified possible joint locations, 42 basic members are identified (Figure 15, (a)). The structural topology graph G with 42 nodes and 66 edges is constructed from the identified basic members (Figure 15, (b)).

As in Figure 16 (a), variable $\boldsymbol{y}_i$ has two elements, $y_{i\,0}$ and $y_{i\,1}$. The first element $y_{i\,0}$ represents the upper/lower thickness of the beam when the beam is placed on the horizontal plane. In this case, the second element $y_{i\,1}$ represents the side thickness of the beam. Similarly, when the beam is placed on the vertical plane, $y_{i\,0}$ represents the front/back thickness of the beam while $y_{i\,1}$ represents the side thickness of the beam.

Figure 16 (b) illustrates the definition of variable z_i, where $z_{i\,0}$ is the thickness of weld between cast and component 0 and $z_{i\,1}$ is the thickness of weld between cast and component 1. Considering the symmetricity, the variables are assigned only to the 21 basic members corresponding to the left half of the boy structure.

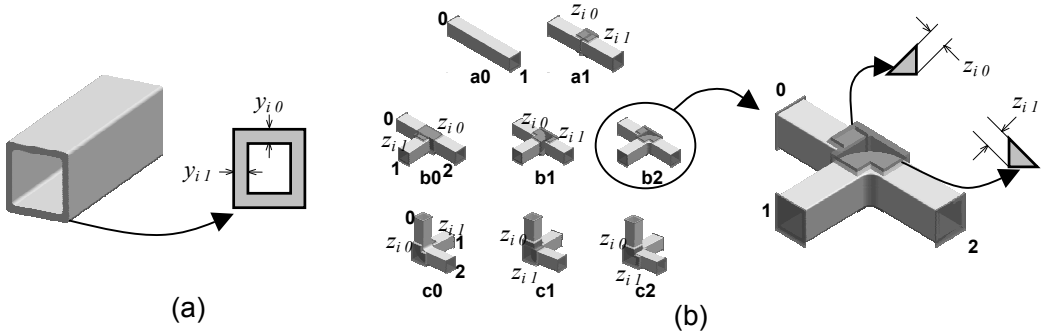

Figure 16: (a) Beam cross sectional design variable and (b) joint design variable.

Stiffness of the assembled structure is calculated considering the maximum displacement of floor frame under bending loads (Figure 17). The main loads of powertrain $\mathbf{F}_{pt}$, the front passengers/seats $\mathbf{F}_{pf}$, the rear passenger/seats $\mathbf{F}_{pr}$, and the luggage $\mathbf{F}_{l}$ are only considered [14], where the magnitude of each load is the weight of the corresponding component multiplied by a dynamic load factor. The rear suspension locations are constrained in x, y, and z translations while the front suspension locations are constrained in z (upward) translation only. Table 2 shows magnitude of the applied loads and the dynamic load factor.

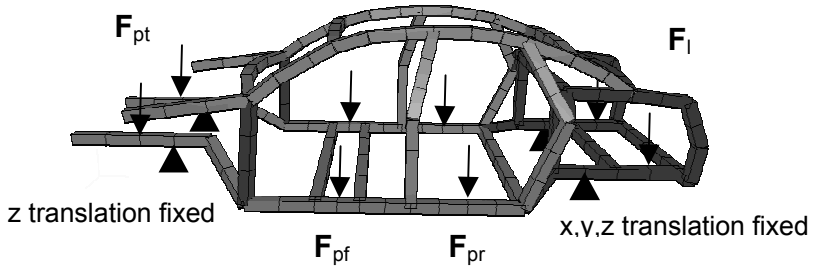

Figure 17: Loading condition and boundary condition [13]

	Default Value*	***Dynamic Factor***	***Applied Value****
$\mathbf{F}_{pt}$	4,000.0	2.0	8,000.0
$\mathbf{F}_{pf}$	1,200.0	2.0	2,400.0
$\mathbf{F}_{pr}$	1,200.0	2.0	2,400.0
$\mathbf{F}_{l}$	500.0	2.0	1,000.0

*Unit [N]

Table 2: Applied load and dynamic load factor (One side)

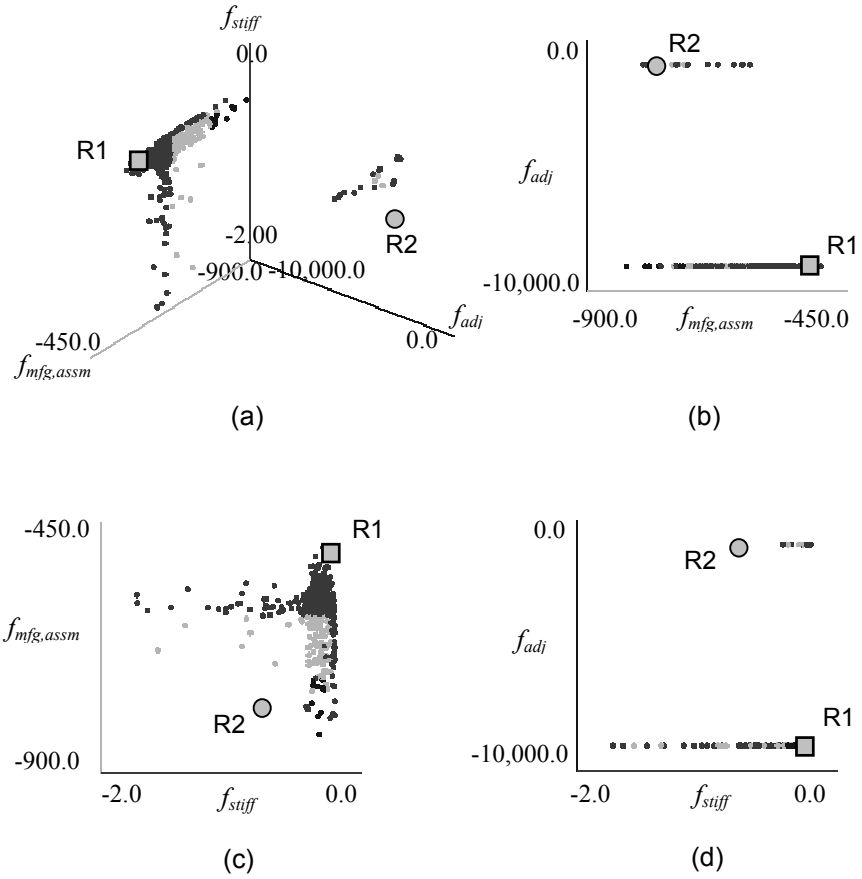

Figure 18: Designs at the terminal condition (generation = 50). Pareto solutions are shaded as black dots.

As a training data for the artificial neural network (ANN) that implements the joint library, the detailed 3D models of 7 joint types (**a1**, **b0**~**b2**, **c0**~**c2**) in Figure 14 (b) are analyzed using finite element analyses. For joint type **a1**, 3 torsional spring rates (x, y, and z components between two joining frames) are calculated. For the other joint types, 9 torsional spring rates (x, y, and z components among three joined frames as shown in Figure 7) are calculated. For each spring rate, a radial-based network [15] is built with 6 input nodes (two $\boldsymbol{y}$'s for two joined frames and one $\boldsymbol{z}$ for the joint), 1,250 hidden layer nodes and 1 output node (joint rate) The networks are trained with newrb function in Matlab [16] to reach a satisfactory convergence (RMS Error < 10%). As the GA parameters, 1,000 populations with 50 number of generation are used in the case study. The number of generation (50) was used as the termination condition. Using a PC with hyper-threaded Pentium 4 3.07 GHz, one optimization run takes approximately 2 days.

Figure 18 illustrates the Pareto solutions at the terminal generation. Figure 18 (a) shows 3-D view of Pareto set and (b) ~ (d) illustrate 2-D space viewed from two selected objects. Two individual designs R1 and R2 are selected and discussed. Design R1 (Figure 19 (a)) shows good results both in stiffness and manufacturing/assembly cost. This structure has long one-piece rocker rails (C_0)

with thick wall dimensions which seem to increase the stiffness of the structure under global bending loading. Also, this design minimizes number of beam components (minimizing extrusion dies) and joint casting components (minimizing number of casting sleeves) by not having joints at location type A (See Figure 14), resulting in minimized manufacturing and assembly cost. However, small number of components limited the adjustable directions to satisfy given 5 KCs, resulting in worse adjustability compared to the design R2.

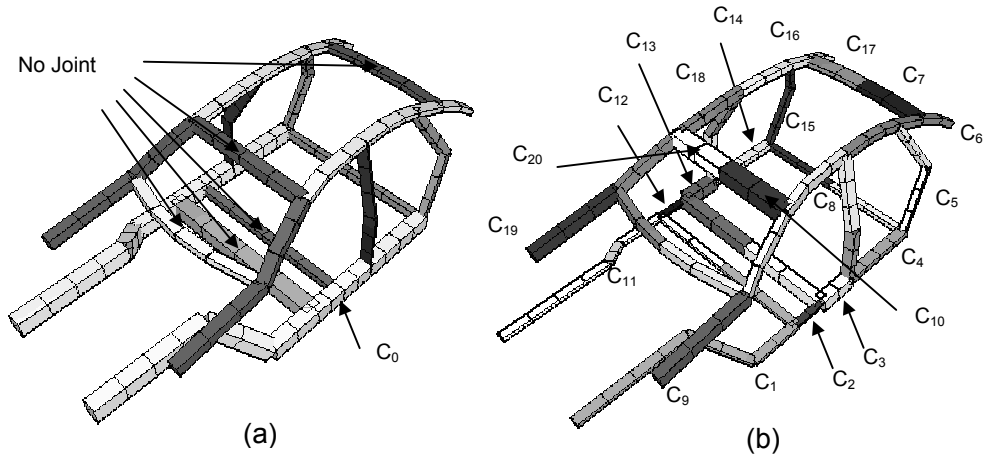

Figure 19: Individual Designs from Pareto Set. (a) R1 and (b) R2.

	# of Comp.	f_{siff} *[mm]*	$f_{mfg,assm}$ *[$]*	f_{adj}
R1	12	**-0.059**	**-496.6**	-10,000.0
R2	20	-0.679	-794.2	**-0.12**

Table 4: Objective function values for Design R1 and R2

Design R2 (Figure 19 (b)) contains relatively thin-walled extrusion components in the rocker (C_1 and C_2) resulting low stiffness of the structure. Also this design contains relatively large number of components (20) which increased the manufacturing cost (by having more extrusion dies) and assembly cost (by having more number of joint locations requiring joining). However the design with a large number of components accompanied by a large number of joints gave more freedom in achieving a very good adjustability that satisfies all 5 KCs almost perfectly. Detailed subassembly partitioning for the design R2 is illustrated in Figure 20. 6 subassemblies of R2 are shown in different colour in Figure 20 (a) and components that comprise the subassembly are listed in Table 5.

The assembly sequence that satisfying all 5 KCs for design R2 is as follows: 1) A and B are assembled to satisfy **KC5**. 2) Then C is assembled to {A,B} in the manner that satisfies **KC3**. 3) In the same way, assembly between D and {A,B,C} is done to satisfy **KC4**. 4) The subassembly E is the mirror image of {A,B,C,D}. Internally, E is built same way of {A,B,C,D}. **KC2** is satisfied by assembling {A,B,C,D} and E. 5) Finally, subassembly F is assembled to {A,B,C,D,E} to satisfy the last KC, **KC1**.

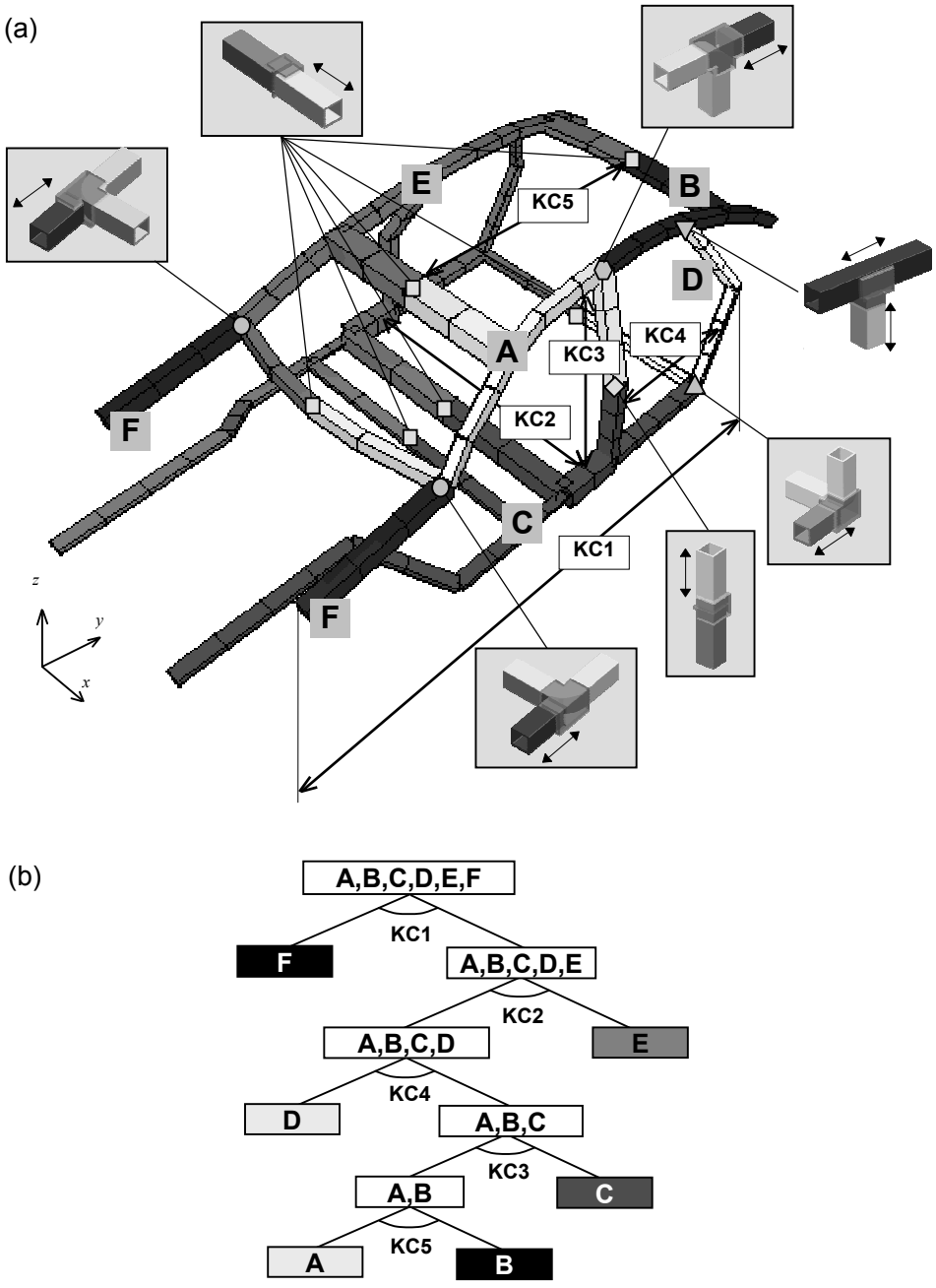

Figure 20: Subassembly partitioning for R2. (a) 6 Subassemblies and (b) binary tree.

Subassemblies	*Components marked in Figure 19*
A	C_8, C_{10}
B	C_6 ~C_7
C	C_1 ~C_4
D	C_5
E	C_{11}~C_{18}, C_{20}
F	C_9, C_{19}

Table 5: Subassemblies for Design R2

5 Conclusion

This paper described a method for synthesizing multi-component structural assemblies of ASF using joint library. First, components set of ASF are parameterized by the joint libraries and transformed into the structural topology graph. Then, the structural topology graph was decomposed by specified joint configurations at each joint locations. By assigning the beam cross sectional design variables and the joint design variables to the decomposed components, the components set of ASF was able to be evaluated considering the stiffness of the assembled ASF, manufacturing/assembly cost and dimensional integrity. Multi-objective optimization algorithms combined with graph-based crossover operator and FE analysis were utilized to solve the given multi-objective optimization problem. As a case study, one of the medium size ASF structure was decomposed into the components set. 2 representative designs in the Pareto set obtained using proposed methods were selected and their design characteristics and trade-offs were discussed.

6 Acknowledgements

The authors acknowledge funding provided by Toyota Motor Corporation and National Science Foundation under CAREER Award (DMI-9984606) for this research. We thank Mr. Karim Hamza at Discrete Design Optimization Laboratory at the University of Michigan for providing his FEM code. Any opinions, findings, and conclusions or recommendations expressed in this material are those of the authors and do not necessarily reflect the views of the National Science Foundation.

References

[1] Yetis, A. and Saitou, K., 2002, “Decomposition-Based Assembly Synthesis Based on Structural Considerations,” ASME Journal of Mechanical Design, vol. 124, pp. 593–601.

[2] Lee, B. and Saitou, K., 2003, "Assembly Synthesis with Subassembly Partitioning for Optimal In-Process Dimensional Adjustability," Proceedings of the 2003 ASME Design Engineering Technical Conferences, Chicago, Illinois, September 2-6, DETC2003/DAC-48729. An extended version is submitted to ASME Journal of Mechanical Design.

[3] Lyu, N. and Saitou, K., 2003, “Decomposition-based assembly synthesis of a 3D Body-In-White for structural stiffness”, Proceedings of the 2003 IMECE, Washington, D.C., Nov 15-21, 2003, IMECE2003-43130. An extended version is accepted to ASME Journal of Mechanical Design.

[4] Lyu, N. and Saitou, K., 2004, “Decomposition-based assembly synthesis of Space Frame structures using Joint library”, Proceedings of the 2004 ASME Design Engineering Technical Conferences, Salt Lake City, Utah, September 28-October 2, DETC2004/DAC-57301

[5] Cetin, O and Saitou, K., 2003, "Decomposition-based assembly synthesis of multiple structures for minimum production cost" Proceedings of the 2003 ASME International Mechanical Engineering Congress and R&D Exposition, Washington, D.C., Nov 15-21, IMECE2003-43085..
[6] Lee, B. and Saitou, K., 2003, "Decomposition-based Assembly Synthesis for In-Process Dimensional Adjustability," ASME Journal of Mechanical Design, vol. 125, pp. 464-473.
[7] Deb., K., Agrawal, S., Pratab, A., and Meyarivan, T., 2000, "A Fast Elitist Non-Dominated Sorting Genetic Algorithm for Multi-Objective Optimization: NSGA-II", KanGAL report 200001, Indian Institute of Technology, Kanpur, India.
[8] Pereira, F., Machado, P., Costa, E., and Cardoso, A., 1999, "Graph Based Crossover – A Case Study with the Busy Beaver Problem", Proceedings of the 1999 Genetic and Evolutionary Computation Conference.
[9] Lyu, N., and Saitou, K., 2003, "Topology Optimization of Multi-component structures via Decomposition-based assembly synthesis", Proceedings of the 2003 ASME DETC, September 2-6, 2003, Chicago, IL., DETC2003/DAC-48730. An extended version is submitted to ASME Journal of Mechanical Design.
[10] Whitney, D. E., Mantripragada, R., Adams, J. D., and Rhee, S. J., 1999, "Designing assemblies," Research in Engineering Design, vol. 11, pp. 229-253.
[11] Long, L., 1998. "Design-oriented Translators for Automotive Joints", Ph.D. Thesis, Virginia Polytechnic Institute.
[12] Ahmetoglu, M. A., "Manufacturing of Structural Automotive Components from Extruded Aluminum Profiles", SAE Technical Paper, 2000-01-2712, International Body Engineering Conference, Detroit, Michigan, Oct 3-5, 2000.
[13] Goldberg E. R., Samtani M. P., "Engineering Optimization via the genetic algorithm". In: 9th conference on Electronic Computation, New York, ASCE, 1986. p. 471-82.
[14] Brown, J. C., et al., 2002. Motor Vehicle Structures: Concept and Fundamentals, SAE International, 2002, pp 68-69.
[15] Chen, S., Cowan, C., and Grant, P. M., "Orthogonal least squares learning algorithm for radial basis function networks," IEEE Transaction on Neural Networks, 1991, vol. 2 (2), pp. 302-309.
[16] Matlab, The language of Technical Computing, Ver. 6.0.0.88, Release 12. The MathWorks, http://mathworks.com